Available online at www.sciencedirect.com
ScienceDirect
Trans. Nonferrous Met. Soc. China 35(2025) 2822−2829
Transactions of Nonferrous Metals Society of China
www.tnmsc.cn

Effects of dislocation loop on microstructure and mechanical properties of LN_2-quenched 2524 Al alloy

Hui YU[1], Li-ping TIAN[1], Li-wei QUAN[1], Chao LIU[1],
Li-xin HUANG[2], Yu-ling XU[3], Wei YU[4], Bin-an JIANG[5], Kwang-seon SHIN[6]

1. Tianjin Key Laboratory of Materials Laminating Fabrication and Interfacial Controlling Technology, School of Materials Science and Engineering, Hebei University of Technology, Tianjin 300130, China;
2. Guangzhou Huitian Intelligence Technology Co., Ltd., Guangzhou 511400, China;
3. Baomarc (Hefei) Technology Co., Ltd., Hefei 238000, China;
4. School of Materials Science and Engineering, Hefei University of Technology, Hefei 230009, China;
5. PLA AAAAD, Hefei 230031, China;
6. Department of Materials Science and Engineering, Seoul National University, Seoul 08826, Korea

Received 16 January 2024; accepted 30 September 2024

Abstract: The microstructure and mechanical properties of 2524 Al alloy after quenching in liquid nitrogen (LN_2) were investigated by TEM and compared with those of cold water quenching. The results show that the LN_2 quenching process effectively induces the formation of dislocation loops. These loops become large and unevenly distribute after aging for 15 min. Furthermore, such loops become rapidly immobilized by the precipitation of coarse *S* phases after 1 h aging. The alloy quenched in LN_2 demonstrates superior peak hardness and displays a more rapid response to subsequent aging treatments compared with the cold water-quenched one. Despite the short aging time, LN_2-quenched sample achieves tensile strength of 488 MPa. This enhanced strength is attributed to the strengthening effect of numerous finely dispersed Guinier-Preston-Bagaryatsky (GPB) zones, in conjunction with the inhomogeneous formation of *S* phase on the dislocation loops.

Key words: 2524 Al alloy; LN_2 quenching; dislocation loop; GPB zone; *S* phase

1 Introduction

Al−Cu−Mg alloys, renowned for their high strength and heat treatability, have emerged as crucial structural materials in the aerospace industry owing to their favorable characteristics such as thermal stability, excellent damage tolerance, and creep resistance [1−4]. The conventional age-hardening heat treatment process for such alloys comprises three primary steps: (1) high-temperature solution treatment, (2) quenching, and (3) aging, allowing precise control over precipitation phenomena [5]. The Al−Cu−Mg alloys usually exhibit quench sensitivity, as their capacity for achieving maximum precipitation hardening is contingent upon the cooling rate employed during the quenching process [6−8].

Generally, the fast quenching rate enhances subsequent precipitation behavior [9−11]. This acceleration allows solute atoms to diffuse belatedly and maintains the high concentration of vacancies

Corresponding author: Hui YU, Tel: +86-18522233466, E-mail: huiyu@vip.126.com;
Li-wei QUAN, Tel: +86-18322608455, E-mail: quanlw@hebut.edu.cn;
Wei YU, Tel: +86-13866723380, E-mail: yuwei52213@163.com
https://doi.org/10.1016/S1003-6326(25)66850-6

in the matrix, preventing their dissipation. Consequently, a high concentration of supersaturated vacancies is retained in such alloy. These vacancies not only facilitate the formation of quenched dislocation loops but also expedite the diffusion of solute atoms during the aging process. Alternatively, they may directly act as nucleation sites for the second phase precipitation, leading to a finer, denser precipitation distribution throughout the process. This process ultimately ensures the attainment of exceptional strength and optimal corrosion resistance through the fastest quenching rate.

In contrast to conventional quenching techniques, liquid nitrogen (LN_2) quenching notably enhances the mechanical properties while reducing residual stress of the materials [12,13]. Theoretically, LN_2 cools approximately five times faster than cold water [5], so the alloy will obtain improved mechanical characteristics after quenching. Upon the solid solution treatment of 2524 Al alloy, the introduction of dislocation loops becomes apparent [8,14]. TIAN et al [15] have demonstrated that the precipitation of secondary phases on these dislocation loops contributes to superior mechanical properties subsequent to quenching in cold water. Unfortunately, in-depth studies concerning quenching media at lower temperatures remain limited. Thus, it becomes imperative to comprehensively explore the microstructural evolution and mechanical properties of aluminum alloy quenched in LN_2. This study aims to ascertain the presence of quenched dislocation loops in LN_2 and to evaluate their potential impact on alloy strength. Moreover, this study aims to elucidate the interplay among quenching rate, dislocation loops, and secondary phases, thereby enhancing the utilization of LN_2 quenching in Al alloy.

2 Experimental

The as-rolled 2524 Al alloy with a nominal composition of Al−4Cu−1.5Mg (in wt.%) was selected to ensure the achievement of meticulous and reliable experimental results. The actual chemical composition determined by inductively coupled plasma (ICP) is presented in Table 1. The 2524 Al sheets underwent heat treatment at 495 °C for 0.5 h, followed by immediate quenching in LN_2. To mitigate the influence of the nitrogen film on the sample surface, adequate cooling was achieved by continuous stirring of the LN_2 for a duration of 2 min. Subsequently, aging was conducted within an oil bath maintained at 170 °C.

Vickers microhardness measurements of the carefully polished samples were carried out using a Shimadzu HMV-G-XY-S microhardness tester with a load of 4.9 N and a loading time of 20 s. The hardness values were averaged over seven consecutive measurements to attain representative data. Room-temperature tensile tests were performed using a UTM5105GD test system at a strain rate of 1 mm/min.

For transmission electron microscopy (TEM) analysis, thin 3 mm-thick discs were prepared by cutting, grinding and punching. These discs were subsequently ion-milled using the PIPS II (GANTAN 695). The TEM observation and characterization were examined by the JEM−2100F operating at an acceleration voltage of 200 kV.

Table 1 Chemical composition of commercial 2524 alloy (wt.%)

Cu	Mg	Mn	Si	Fe	Zn	Mo	Al
4.21	1.38	0.75	0.42	0.07	0.02	0.02	Bal.

3 Results and discussion

3.1 Hardness and peak-aged room temperature tensile properties of LN_2-quenched alloy

Figure 1(a) illustrates the evolution of Vickers hardness for 2524 Al alloy subsequent to quenching in LN_2 and cold water, respectively, followed by aging at 170 °C. The plots show similar aging trends for both quenched alloys, with the LN_2-quenched alloy showing not only a higher peak hardness but also a more rapid response to peak aging. Our previous research [15] has shown that the cold water-quenched alloy reaches a peak hardness of HV 140 after 72 h of aging. In contrast, the LN_2-quenched alloy achieves a peak hardness of HV 149 after only 48 h of aging, clearly demonstrating the significant increase in hardness achieved by LN_2 quenching. In addition, the LN_2 quenching approach significantly reduces the aging time required to achieve peak hardness.

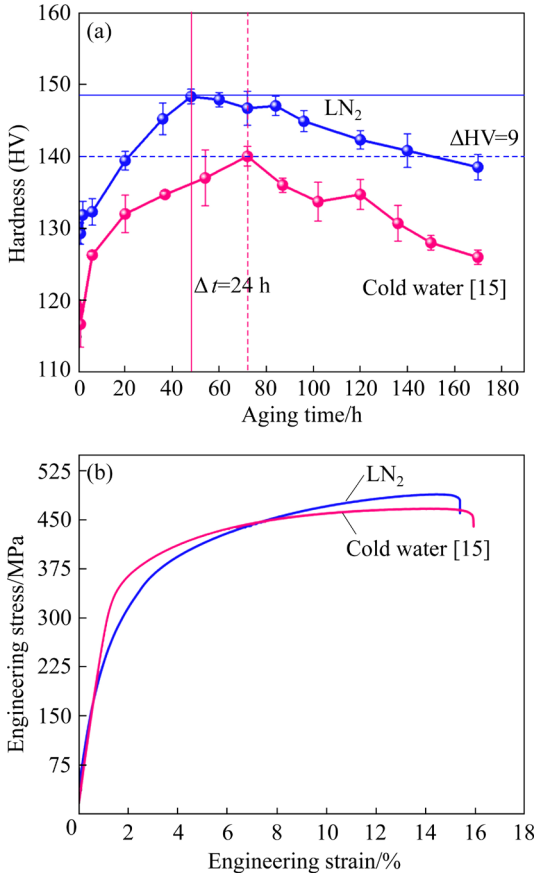

Fig. 1 (a) Age-hardening curves of 2524 alloy cooled in LN_2 and cold water versus aging time; (b) Engineering stress−strain curves of two quenched alloys at peak aging

Figure 1(b) shows the representative engineering stress−strain curves obtained from the peak aging stage for both LN_2-quenched and cold water-quenched alloys. It is evident from the figure that while the tensile yield strength (TYS) and elongation (EL) of the LN_2-quenched alloy experience a slight reduction compared with the cold water-quenched counterpart, the ultimate tensile strength (UTS) is comparable or even slightly increased, reaching 488 MPa in a short aging duration. The comprehensive mechanical properties of the two quenched alloys are listed in Table 2. This observation aligns with the findings depicted in Fig. 1(a), indicative of the influence of aging hardening. A plausible explanation lies in the practice of continuous stirring during LN_2 quenching, which minimizes the influence of nitrogen film on the alloy surface, thereby facilitating a greater cooling rate in LN_2 than that achieved in cold water. These findings collectively testify the capacity of LN_2 quenching to effectively enhance the strength and hardness of the aluminum alloy, contradicting previous research conclusions [16].

Table 2 Mechanical properties of two quenched alloys in peak aging state at room temperature

Sample	TYS/MPa	UTS/MPa	EL/%
Cold water-quenched	336.2±2.2	467±1.5	16±2.6
LN_2-quenched	211.6±2.6	488±3.2	15.4±1.3

3.2 Characteristics of dislocation loops and precipitates

The microstructure of the alloy quenched in LN_2 at various aging stages was characterized using TEM to investigate the underlying factors contributing to the observed increase in both strength and hardness. Figure 2 shows the TEM images of the alloy after quenching in LN_2. As can be seen from Figs. 2(a−c), the presence of dislocation loops and *S* phases in the quenched state of the alloy is not observed either from the $[110]_{Al}$ or $[100]_{Al}$ direction before artificial aging, and the fast Fourier transform (FFT) image shown in Fig. 2(d) confirms that there is no *S* phase precipitation in the alloy at this state.

Figure 3 presents the microstructure of the LN_2-quenched alloy near the $[110]_{Al}$ or $[100]_{Al}$ axis during the initial stage of aging. The yellow circles and the red squares/arrows in Fig. 3 represent the dislocation loops and the *S* phases precipitated on these loops, respectively. After aging for 15 min, a notable presence of dislocation loops similar to those observed in the cold water-quenched alloy appears in the LN_2-quenched counterpart [15]. However, these loops have larger dimensions as well as uneven distribution, as shown in Figs. 3(a, b). This phenomenon can be attributed to the extremely rapid cooling rate of the LN_2-quenched sample, which induces high thermal stresses and quenching deformations, resulting in high dislocation density. Subsequently, during the aging process, the pre-existing dislocation lines, acting as strong defects, exert a significant influence on the nucleation and evolution of dislocation loops. These dislocation lines effectively reduce the concentration of point defects generated during quenching, thereby facilitating the growth of dislocation loops while suppressing their nucleation [17,18]. Consequently, at the initial

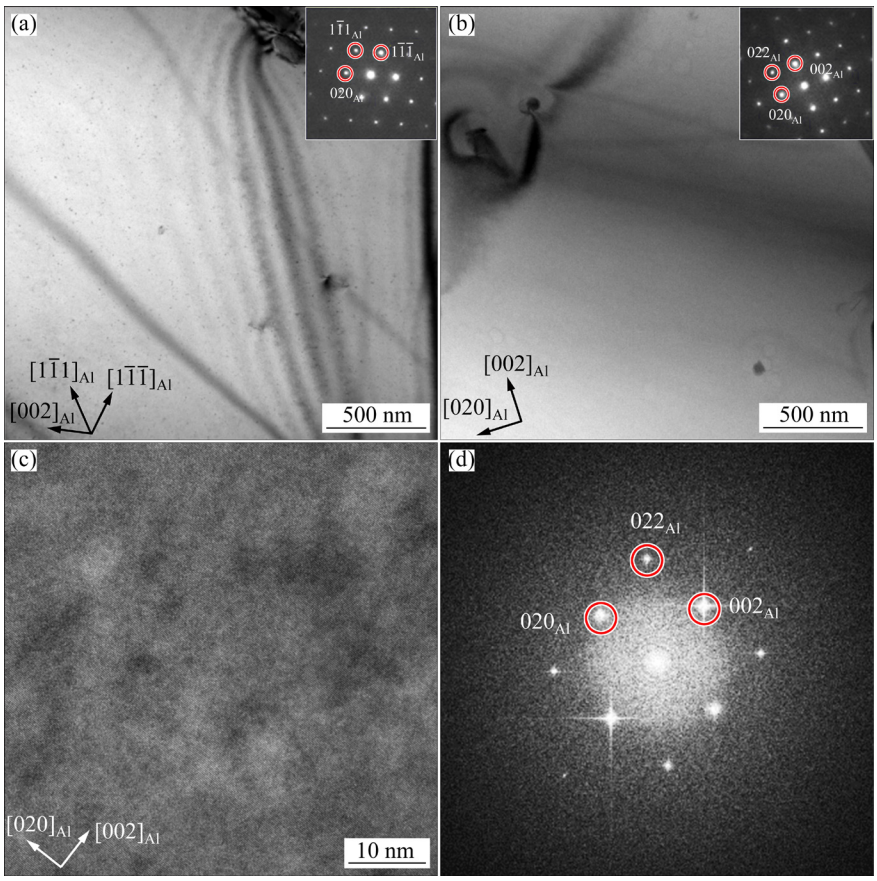

Fig. 2 TEM images of LN_2-quenched Al alloy: (a) B=$[110]_{Al}$; (b) B=$[100]_{Al}$; (c) HRTEM image; (d) FFT pattern (The insets show the corresponding SADP)

stage of aging, the number of dislocation loops remains limited, but their sizes are enlarged.

Moreover, the rapid cooling rate enables the Al alloy to acquire a substantial amount of supersaturated solute atoms and vacancies. However, the presence of dislocation lines accelerates the growth of dislocation loops by facilitating their absorption of surrounding supersaturated vacancies or the formation of new loops through the intersection and merging of existing dislocation loops. This dynamic process leads to the disappearance of the original dislocation loops and the formation of large ones. Consequently, the density of these loops diminishes, and their shapes become irregular, thereby explaining the observed variations in loop size and imperfect elliptical shapes observed in Figs. 3(a, b).

Small precipitates were also found within the sample (see Fig. 3(c)). A high-resolution transmission electron microscopy (HRTEM) examination, shown in Fig. 3(d), corroborated by the corresponding FFT image, confirmed these precipitates as S phases [19,20], which play a crucial role in strengthening the alloy throughout the thermal aging process [21,22].

Upon aging for 1 h, the dislocation loops within the alloy become indiscernible, attributed to their coarsening and the entanglement effect resulting from the growth of S phases on them. Figures 3(e−h) exemplify this transition, as the loops are supplanted by numerous coarse S phases. The scanning transmission electron microscopy (STEM) image presented in Fig. 3(e) offers a clear view of the morphology and distribution of these coarsened S phases. Additionally, the HRTEM image in Fig. 3(h) reveals a noticeable increase in the thickness of the S phase due to aging, ranging from 2−4 atomic layers to 6−8 atomic layers. This accounts for the rapid increase in hardness observed during the under-aging stage in Fig. 1(a), as a substantial volume of enlarged strengthening S phases is generated. This experimental finding corroborates previous research, which indicates that the size of S phases adhering to dislocation loops magnifies during the beginning of aging [15].

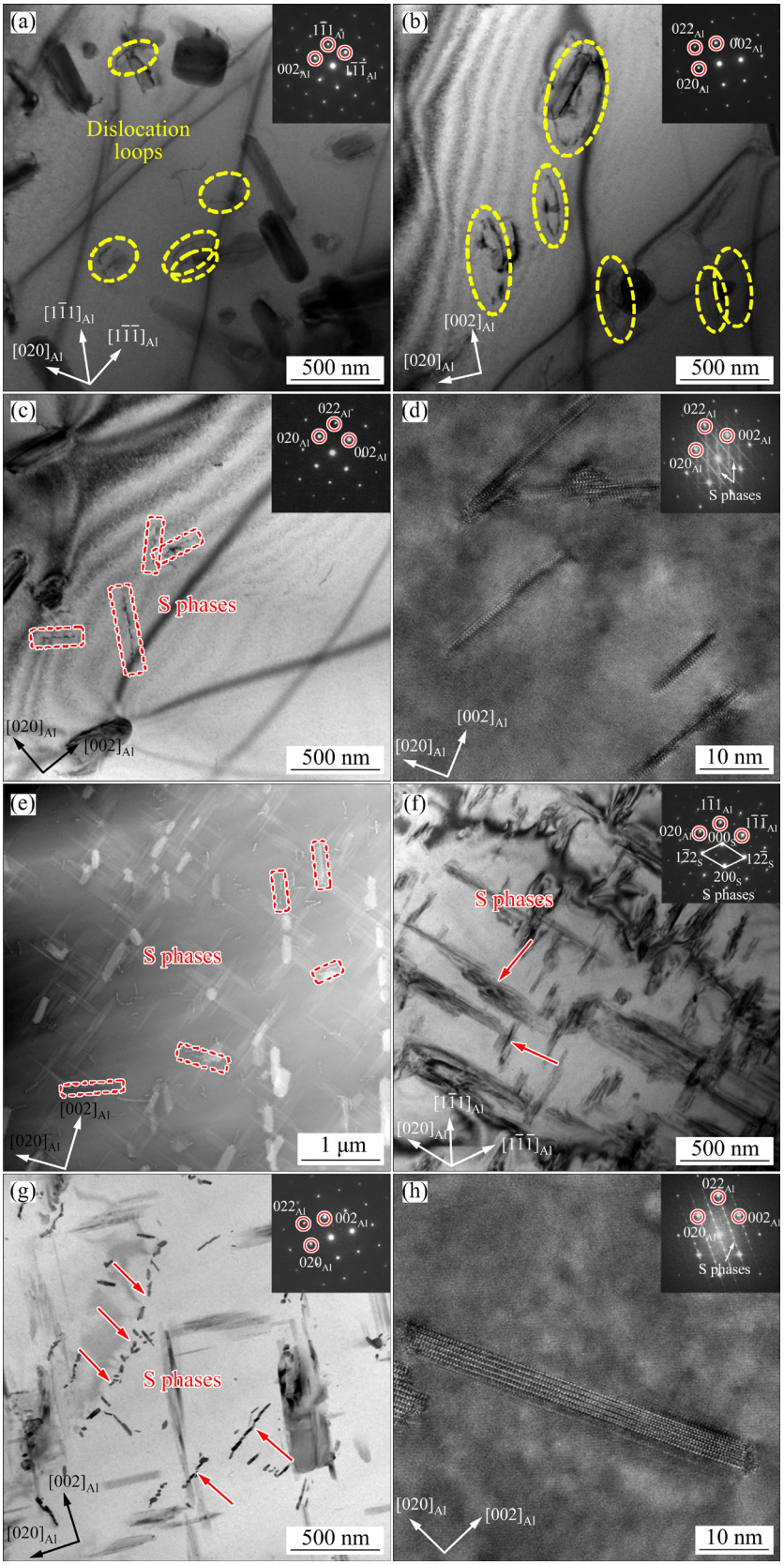

Fig. 3 TEM images of alloy aged at 170 °C for 15 min (a−d) and for 1 h (e−h) after cooling in LN_2: (a, b) Dislocation loops viewed from $[110]_{Al}$ and $[100]_{Al}$ zone axes, respectively; (c) Low-magnification image of *S* phase; (d) HRTEM image of *S* phase; (e) HADDF-STEM image of *S* phase; (f, g) *S* phase morphology viewed from $[110]_{Al}$ and $[100]_{Al}$ zone axes, respectively; (h) HRTEM image of *S* phase (The insets are the corresponding SADP or FFT patterns of interesting regions)

Significantly, in contrast to the alloy cooled in cold or boiling water wherein visible dislocation loops persist and grow during aging, the LN_2-quenched alloy, when aged for 1 h, exhibits the absence of observable dislocation loops due to the presence of coarse *S* phases that have formed on them. This behavior can be attributed to the instantaneous cooling of the quenched alloy from a high solid solution temperature to −196 °C, resulting in substantial temperature differentials that induce lattice shrinkage and distortion [23,24]. Consequently, the lattice shrinkage and distortion impede dislocation slip, thereby increasing the strength of the alloy [25]. Furthermore, lattice distortion augments the potential energy, thus increasing the density of defects such as vacancies and dislocation nodes, thereby promoting precipitation during aging [24,26]. Consequently, a considerable population of significantly coarsened *S* phases is observed within a relatively short aging period of 1 h.

Figure 4 shows the TEM images of the alloy during the peak aging period. In comparison to Fig. 3, the *S* phases exhibit a noteworthy increase in size, reaching a thickness exceeding 22−26 atomic layers (see Fig. 4(c)). Additionally, a significant occurrence of diffusely distributed, smaller Guinier-Preston-Bagaryatsky (GPB) zones in 1−2 nm, denoted by yellow circles, becomes apparent, as illustrated in Figs. 4(d−f). GPB zones also serve as potent strengthening particles, capable of obstructing dislocation movement and enhancing the overall mechanical properties. They can also form concurrently with the reinforcing *S* phases and interact with each other in terms of microstructure and morphology [27]. Although GPB zones are also present in the cold water-quenched alloy during the peak aging stage, their quantity is far lower, resulting in a comparably weaker strengthening effect on the alloy compared to the *S* phases [15].

In this investigation, the utilization of LN_2 as a quenching medium resulted in the presence of a greater number and larger size of strengthening *S* phases, as well as a densely populated and widely dispersed collection of GPB zones within the alloy. These GPB zones, together with the coarser *S* phases, collectively contribute to the strengthening of the alloy, with GPB zones playing a dominant role. The alloy experiences a substantial temperature range when rapidly transitioning from a high solid solution temperature to LN_2. The continuous stirring of the liquid serves to mitigate the influence

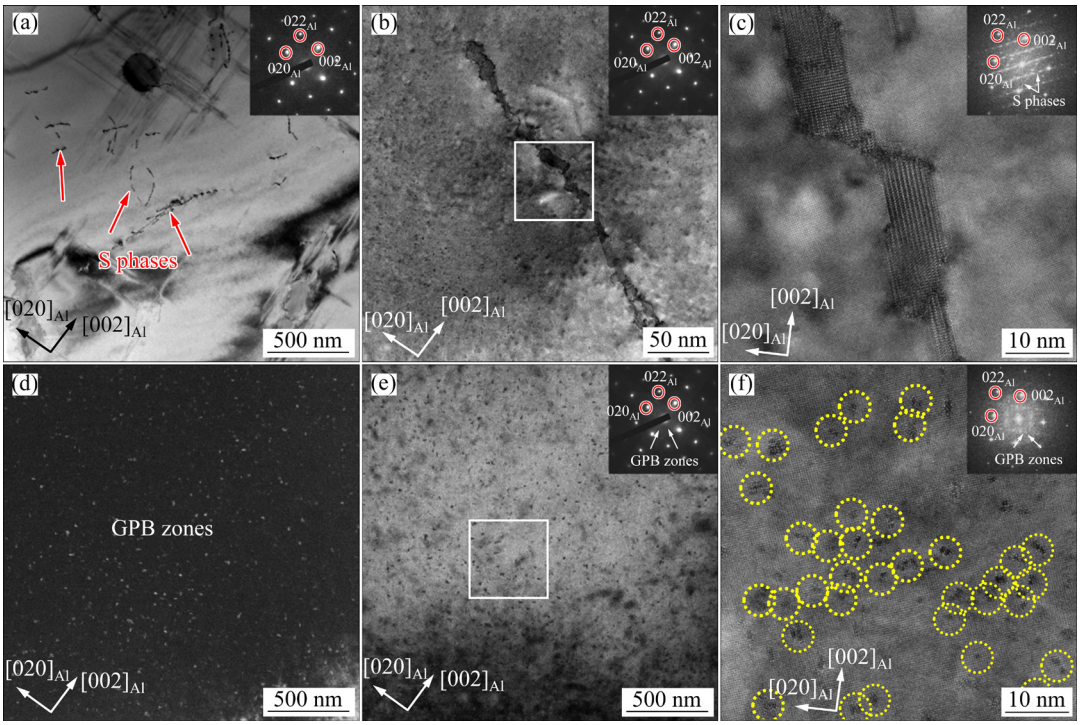

Fig. 4 TEM images of alloy at peak aging state after quenching in LN_2: (a−c) *S* phases; (d−f) GPB zones: (a) Bright-field image of *S* phase; (b) High-resolution image of *S* phase; (c) Local magnification of (b); (d) Dark-field image of GPB zones; (e) Bright-field image of GPB zones; (f) High-resolution images of GPB zones (The insets are the corresponding SADP with B=[100]$_{Al}$ and FFT patterns for the phase analysis)

of the nitrogen film on the alloy surface, thereby significantly accelerating the cooling rate and augmenting the concentration of supersaturated solid solution within the alloy. Consequently, an increased abundance of supersaturated vacancies ensues.

During the early stage of aging, the formation of large dislocation loops with an uneven distribution is observed, which subsequently facilitates the rapid precipitation of *S* phases distributed along these loops. Simultaneously, the concentration of supersaturated solute atoms within the alloy increases, promoting the formation of numerous small and dispersed GPB zones. Through the combined influence of GPB zones and S phases, the aging heat treatment response of the material is substantially enhanced, resulting in comparable or even higher levels of strength and hardness when compared to cold water quenching, in a shorter aging time.

4 Conclusions

(1) Quenched dislocation loops with significant dimension and non-uniform distribution persist in the LN_2-quenched alloy. However, their observability is precluded due to the rapid anchoring effect caused by the precipitation of *S* phases onto the loops after aging for 1 h.

(2) The LN_2-quenched alloy exhibits an acceleration in peak aging, resulting in significant improvements in both hardness and tensile strength.

(3) In addition to the inhomogeneously nucleated *S* phases on dislocation loops, a considerable population of diffuse and small GPB zones precipitate in the alloy during the peak aging. These GPB zones play a prominent role in enhancing the overall strength of such alloy.

CRediT authorship contribution statement

Hui YU: Methodology, Data curation, Formal analysis, Investigation, Writing − Original draft, Writing − Review & editing, Supervision, Project administration; **Li-ping TIAN:** Methodology, Data curation, Formal analysis, Investigation, Writing − Original draft, Writing − Review & editing; **Li-wei QUAN:** Data curation, Formal analysis, TEM analysis; **Chao LIU** and **Li-xing HUANG:** Data curation; **Yu-ling XU:** Writing − Review & editing; **Wei YU:** Formal analysis, Methodology; **Bin-an JIANG:** Data curation; **Kwang-seon SHIN:** Writing − Review & editing.

Declaration of competing interest

The authors declare that they have no known competing financial interests or personal relationships that could have appeared to influence the work reported in this paper.

Acknowledgments

This work was supported by the National Natural Science Foundation of China (No.52001106), and the Natural Science Foundation of Hebei Province, China (No. E2022202158).

References

[1] LI Shuang-shuang, YUE Xin, LI Qing-yuan, PENG He-li, DONG Bai-xin, LIU Tian-shu, YANG Hong-yu, FAN Jun, SHU Shi-li, QIU Feng, JIANG Qi-Chuan. Development and applications of aluminum alloys for aerospace industry [J]. Journal of Materials Research and Technology, 2023, 27: 944−983.

[2] YU Tao, LI Feng, WANG Ye, LI Xue-wen. New powder metallurgy preparation method of homogeneous and isomeric Al−Cu−Mg mixed crystal materials [J]. Transactions of Nonferrous Metals Society of China, 2023, 33: 371−382.

[3] FAN Cai-he, OU Ling, HU Ze-yi, YANG Jian-jun, CHEN Xi-hong. Re-dissolution and re-precipitation behavior of nano-precipitated phase in Al−Cu−Mg alloy subjected to rapid cold stamping [J]. Transactions of Nonferrous Metals Society of China, 2019, 29: 2455−2462.

[4] HAN Feng, HAN Hua, ZHANG Yu, YUAN Tao, WANG Cai-mei. Formation mechanism of the quasicrystal in Al−Cu−Mg−Zn aluminum alloy resistance spot weld [J]. Materials Letters, 2023, 350: 134949.

[5] MACKENZIE D S. Aluminum science and technology: Metallurgy of heat treatable aluminum alloys [M]. Materials Park, OH: ASM International, 2018: 133−152.

[6] MILKEREIT B, WANDERKA N, SCHICK C, KESSLER O. Continuous cooling precipitation diagrams of Al−Mg−Si alloys [J]. Materials Science and Engineering: A, 2012, 550: 87−96.

[7] MILKEREIT B, STARINK M J. Quench sensitivity of Al−Mg−Si alloys: A model for linear cooling and strengthening [J]. Materials & Design, 2015, 76: 117−129.

[8] SHI S, BEI H B, ROBERTSON I M. Impact of alloy composition on one-dimensional glide of small dislocation loops in concentrated solid solution alloys [J]. Materials Science and Engineering: A, 2017, 700: 617−621.

[9] MA Zhi-min, ZHANG Yong, LIU Sheng-dan, DENG Yun-lai, ZHANG Xin-ming. Quenching sensitivity and heterogeneous precipitation behavior of AA7136 alloy [J]. Transactions of Nonferrous Metals Society of China, 2021, 31(11): 3356−3369.

[10] XI Zhu-cong, HECTOR L G, MISRA A, QI Liang. Kinetic Monte Carlo simulations of solute clustering during quenching and aging of Al−Mg−Zn alloys [J]. Acta Materialia, 2024, 269: 119795.

[11] WANG Yi-chang, WU Xiao-dong, YUE Lu, GUO Ming-xing, CAO Ling-fei. Aging precipitation behavior and properties of Al−Zn−Mg−Cu−Zr−Er alloy at different quenching rates [J]. Transactions of Nonferrous Metals

Society of China, 2022, 32(4): 1070−1082.
[12] KUMAR S D, MAGARAJAN U, KUMAR S S, RODRÍGUEZ-MILLÁN M. Effect of deep cryogenic treatment on the microstructural, mechanical and ballistic properties of AA7075-T6 aluminum alloy [J]. Defence Technology, 2023, 30(12): 101−110.
[13] DHARANI K S, SURESH K S. Effect of heat treatment conditions and cryogenic treatment on microhardness and tensile properties of AZ31B alloy [J]. Journal of Materials Engineering and Performance, 2023, 32(19): 8786−8794.
[14] MA K, DÉCAMPS B, HUANG L Z, SCHÄUBLIN R E, LÖFFLER J F, FRACZKIEWICZ A, NASTAR M, PRIMA F, LOYER-PROST M. Impact of micro-alloying in ion-irradiated nickel: From the inhibition of point-defect cluster diffusion by thermal segregation to the change of dislocation loop nature [J]. Acta Materialia, 2023, 246: 118656.
[15] TIAN L P, QUAN L W, WANG C C, YU W, HUANG L X, SHIN K S, YU H. Microstructure and mechanical properties of 2524 aluminum alloy with dislocation loops by various quenching rates [J]. Materials Science and Engineering: A, 2023, 886: 145659.
[16] LISCIC B, TENSI H M, CANALE L C, TOTTEN G E. Quenching theory and technology: Quenching of aluminum alloy [M]. Boca Raton: CRC Press, 2018: 43−84.
[17] WANG Ji-peng, GUO Li, LUO Jin-ru, SONG Jiang-feng, SHI Yan, CHEN Chang-an. In-situ TEM investigation of dislocation loop evolution in HR3 steel during Fe+ ion irradiation [J]. Journal of Nuclear Materials, 2023, 578: 154309.
[18] YANG Gang, WU Yu-kun, DING Yi-fan, LI Yi-peng, CAO Zi-qi, LI Gang, CUI De-wang, HE Kun, QIU Xi, RAN Guang. Effect of ion flux on one-dimensional migration of dislocation loops in Fe9Cr1.5W0.4Si F/M steel during in-situ Fe+ irradiation [J]. Journal of Nuclear Materials, 2023, 579: 154412.
[19] WANG S C, STARINK M J. Precipitates and intermetallic phases in precipitation hardening Al−Cu−Mg−(Li) based alloys [J]. International Materials Reviews, 2005, 50: 193−215.
[20] FENG Z Q, YANG Y Q, HUANG B, LUO X, LI M H, HAN M, FU M S. Variant selection and the strengthening effect of S precipitates at dislocations in Al−Cu−Mg alloy [J]. Acta Materialia, 2011, 59: 2412−2422.
[21] QUAN Li-wei, ZHAO Gang, GAO S, MUDDLE B C. Effect of pre-stretching on microstructure of aged 2524 aluminium alloy [J]. Transactions of Nonferrous Metals Society of China, 2011, 21: 1957−1962.
[22] LIU Yu-ying, HAN Xiang-bin, WANG Shuang-bao, WEI Bo, LI Wei-zhou. Subtle atomistic processes of S-phase formation in Al−Cu−Mg alloys [J]. Journal of Alloys and Compounds, 2020, 838: 155677.
[23] YUAN Chao, WANG Yun-peng, SANG De-li, LI Yi-jun, JING Lei, FU Rui-dong, ZHANG Xiang-yi. Effects of deep cryogenic treatment on the microstructure and mechanical properties of commercial pure zirconium [J]. Journal of Alloys and Compounds, 2015, 619: 513−519.
[24] WENG Ze-ju, XU Xia-fan, YANG Biao, GU Kai-xuan, CHEN Liu-biao, WANG Jun-jie. Cryogenic thermal conductivity of 7050 aluminum alloy subjected to different heat treatments [J]. Cryogenics, 2021, 116: 103305.
[25] WANG C Y, CEPEDA-JIMÉNEZ C M, PÉREZ-PRADO M T. Dislocation-particle interactions in magnesium alloys [J]. Acta Materialia, 2020, 194: 190−206.
[26] DINESH S, SENTHILKUMAR V, ASOKAN P, ARULKIRUBAKARAN D. Effect of cryogenic cooling on machinability and surface quality of bio-degradable ZK60 Mg alloy [J]. Materials & Design, 2015, 87: 1030−1036.
[27] YIN Mei-jie, CHEN Jiang-hua, WANG Shuang-bao, LIU Zi-ran, CHA Li-mei, DUAN Shi-yun, WU Cui-lan. Anisotropic and temperature-dependent growth mechanism of S-phase precipitates in Al−Cu−Mg alloy in relation with GPB zones [J]. Transactions of Nonferrous Metals Society of China, 2016, 26: 1−11.

位错环对液氮淬火 2524 铝合金显微组织与力学性能的影响

余 晖[1]，田丽平[1]，权力伟[1]，刘 超[1]，黄礼新[2]，徐玉棱[3]，余 炜[4]，蒋滨安[5]，Kwang-seon SHIN[6]

1. 河北工业大学 材料科学与工程学院，天津市材料层状复合与界面控制技术重点实验室，天津 300130；
2. 广州汇天智能科技有限公司，广州 511400；
3. 宝玛克(合肥)科技有限公司，合肥 238000；
4. 合肥工业大学 材料科学与工程学院，合肥 230009；
5. 中国人民解放军陆军炮兵防空兵学院，合肥 230031；
6. Department of Materials Science and Engineering, Seoul National University, Seoul 08826, Korea

摘 要：利用透射电子显微镜(TEM)研究液氮(LN_2)淬火与冷水淬火条件下 2524 铝合金的显微组织与力学性能差异。结果表明，LN_2 淬火能够有效诱导位错环形成，时效 15 min 后位错环尺寸增大且分布不均匀；继续时效至 1 h 时，粗化 *S* 相迅速钉扎位错环。与冷水淬火相比，LN_2 淬火合金峰值硬度更高且时效响应速度更快。此外，LN_2 淬火合金在较短时效时间内可实现 488 MPa 抗拉强度。该强度提升主要归因于大量弥散分布、尺寸细小的 Guinier-Preston-Bagaryatsky(GPB)区与 S 相在位错环上非均匀析出的协同强化作用。

关键词：2524 铝合金；液氮淬火；位错环；GPB 区；S 相

(Edited by Xiang-qun LI)